PAPER • OPEN ACCESS

Case-based reasoning user support for industrial x-ray computed tomography

To cite this article: Leonard Schild *et al* 2023 *Meas. Sci. Technol.* **34** 045403

View the article online for updates and enhancements.

You may also like

Case-based reasoning user support for industrial x-ray computed tomography

Leonard Schild[1,*] , **Katja Höger**[1,*] , **Filippo Zanini**[2], **Gisela Lanza**[1,3] **and Simone Carmignato**[2,3]

[1] wbk Institute of Production Science, Karlsruhe Institute of Technology (KIT), Karlsruhe, Germany
[2] Department of Management and Engineering, University of Padua, Vicenza, Italy

E-mail: Katja.Hoeger@kit.edu

Abstract

Industrial x-ray computed tomography is increasingly used in the field of dimensional metrology. However, the measurement accuracy is influenced by many factors for which comprehensive expert's knowledge is still not available. This work presents an approach to establish a user support system that allows a user to achieve highly accurate measurements. The approach generates knowledge from experimental investigations deploying specifically designed test parts and uses the knowledge in a case-based reasoning user support system. Validation experiments showed that the user support system was successful at providing a user with instructions that led to highly accurate measurements of three previously unknown industrial workpieces.

(Some figures may appear in colour only in the online journal)

1. Introduction

The following introduction explains why case-based reasoning (CBR) is introduced as a promising concept for a computed tomography (CT)-focused user support system.

1.1. User support systems

Industrial x-ray CT is increasingly used for conducting dimensional measurements of industrial workpieces [1, 2]. Optimizing the choice of scan parameters is a fundamental aspect to enable accurate measurements [3]. However, choosing the scan parameters is not trivial and still strongly based on user experience. Different users typically apply different optimization strategies that can lead to varying results for the same measurement task, as demonstrated by interlaboratory comparisons [4, 5]. To overcome this hurdle, user support systems have been proposed in literature.

Schmitt *et al* [6] presented a knowledge-based user support system. The system helps users to choose scan parameters relating to the x-ray source as well as the number of projections and the projections' integration time. The system relies on ray-tracing simulations to optimize the scan parameters for previously unknown workpieces.

Buratti *et al* [7, 8] and Schmitt *et al* [9] continued the initial work of Schmitt *et al* [6]. They concentrated on improving the presented ray-tracing model by enabling it to represent multi-material workpieces. Key to the improvement was a physically inspired model that optimizes the x-ray spectrum. So far, the user support system's abilities were tested only with a single, specially developed test part.

Kraemer *et al* [10] presented an approach that relies on optimizing the image quality of x-ray projections. This approach does not need any previous information regarding
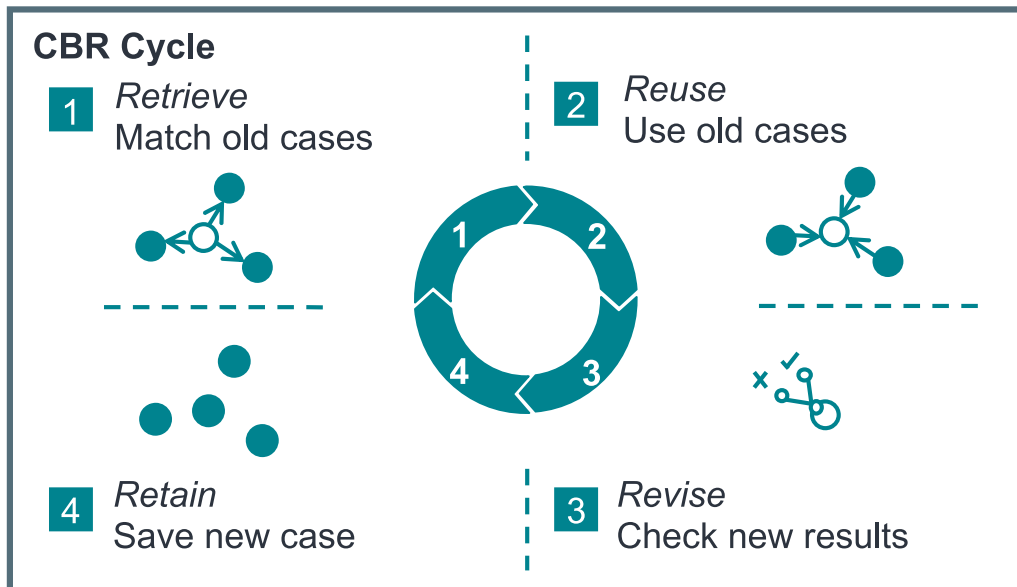

Figure 1. Visualization of the CBR cycle's four steps.

the workpieces' shapes. In their work, they presented a selection of suitable image quality parameters to quantify image quality.

Christoph *et al* [11] established a simulation-based user support system. This system uses deterministic simulations to optimize image quality and subsequentially the single point uncertainty. In a secondary step, the system sets the number of projections and projections' integration time. The approach was tested on a typical sphere forest artifact.

Additional works on user support have been published. For example, Reising *et al* [12], Reiter *et al* [13], Xue *et al* [14] and Schielein *et al* [15] used simulations in which the image quality was optimized. Giedl-Wagner *et al* [16] investigated the applicability of neural networks for user support. These works have in common that they are in a comparatively early stage of development.

The presented user support systems are prototypes that in most cases still need to be validated by testing them with different, industrial workpieces. Moreover, they are mostly based on detailed information on the CT device and/or the workpiece shape in form of 3D models. Especially simulations need to be parameterized correctly to accurately represent a CT device. However, this is often difficult or not possible for typical users of CT devices. Therefore, we introduce the concept of CBR as an alternative concept for a user support system. We propose this concept because it allows to directly derive the user support system from experimental results, which can be more easily adapted by other CT users to their respective CT systems.

1.2. CBR

CBR systems are a specific type of knowledge-based system [17, 18]. Knowledge-based systems provide users with knowledge stored in their database. Typically, they provide knowledge to give advice on how to solve a certain, difficult problem, which is why they are often referred to as expert systems. Of note, in this paper, we called CT-specific expert systems that provide aid to a CT user in regard to the choice of scan parameters 'user support systems'.

CBR systems were developed to improve early knowledge-based systems which relied on a set of fixed rules and were therefore inflexible. In resemblance of how the human brain stores information, CBR systems incorporate knowledge gained from experience in form of cases [18]. Information associated to a case, like a specific patient's treatment to an illness, can be provided by a CBR system to a user to solve a similar problem. Cases are labeled and identified by so-called 'identifying attributes', e.g. information on a patient's age.

A CBR system is based on the so-called CBR cycle, consisting of the following four steps which are visualized in figure 1 [18]:

(a) Retrieve: To solve a new case, the CBR system identifies suitable old cases by comparing the identifying attributes of old cases to the new case's values of these attributes.

(b) Reuse: The CBR system reuses knowledge stored in the old cases to solve the task associated to the new case. How the knowledge is reused, is unique to a specific CBR system's design.

(c) Revise: The CBR system evaluates the results from reusing the old cases' knowledge to solve the new case. Often, the evaluation is carried out by a human expert. If the evaluation shows that the results have been unsatisfactory, other old cases or other means must be used to solve the new case.

(d) Retain: If the results have been satisfactory, the new case is included in the system among the other cases. By adding new cases, a CBR system constantly improves and evolves.

Being directly based on practical experience, a CBR system shows advantages compared to other expert systems. In context of CT-based metrology, the results from past experiments can be directly converted to the CBR system's cases without a need for additional information on the CT device. Further, new results can be continuously incorporated in the CBR system by storing them as additional cases, and thus improve the CBR system itself.

1.3. Establishing a CBR user support system

To evaluate if the CBR approach is particularly well-suited to CT applications, we experimentally established a CBR user-support system in two steps:

(a) First, we performed experiments to generate a knowledge database (section 2) and
(b) Second, we created a CBR user-support system from the knowledge database (section 3).

In step (a), we aimed to generate a comprehensive knowledge database as a foundation for step (b)'s CBR system. To achieve this goal, we manufactured specifically designed test parts in different materials and sizes and measured them with systematically varied scan parameters. We analyzed the measurement results to understand which scan parameters most influence the measurements' accuracy.

In step (b), we aimed to set up a CBR user support system that performs well for most workpieces that are typical for the used CT device. To achieve this goal, we used our understanding of the relationship of the scan parameters and the accuracy gained from the experimental results from step (a) to establish a CBR system as a software tool. Using the tool and specific validation parts, we were able to show that the experimental results-based CBR system allowed us to achieve accurate measurement results for different, representative workpieces.

Figure 2 shows these steps and provides an overview over our approach. The following sections correspond to the overview figure's numbers to make the paper easier to follow.

All experiments were performed with a Zeiss METRO-TOM 800 CT device (max. voltage 130 kV) operating MET-ROTOM OS 3.2 (Zeiss, Germany). Evaluation was carried out with VGStudio Max 3.4 (Volume Graphics, Germany) and MATLAB 2020b (Mathworks, USA).

2. Perform experiments to create knowledge database (figure 2, I)

2.1. Manufacture test parts (figure 2, I.1)

We used six test parts for the experiments which we manufactured in different sizes and materials (figure 3). We chose the parts' sizes and materials to represent workpieces which are typical of the used CT device in terms of the magnifications and penetration lengths. Accordingly, we manufactured three 5 mm test parts made of polyetheretherketon

(Pe, Variante 1000), aluminum (Al, AlMg4.5Mn0.7) and steel (St, 42CrMo4) as well as two 30 mm test parts made of Pe and Al as well as one 100 mm test part made of Pe. To ensure (tactile) measurability of all features, the 5 mm versions had two holes on the top instead of three.

The test part's simple geometry allowed us to deploy high-precision manufacturing processes and tactile reference measurements characterized by low measurement uncertainty. Due to their simple form, the test parts' materials and sizes could also be adopted to requirements of different CT devices.

Figure 4 schematically shows the test part's measurement features for registration, bi-directional and uni-directional measurements. Dimensions are provided in table 1.

We designed the test parts in order to evoke large differences in ray-penetration length in single projections as well as when being rotated. This results in varying wall-thickness and strong anti-rotational symmetry, respectively. Thus, the test parts promote the presence of imaging artefacts in CT reconstructions. Since imaging artefacts can affect the measurement accuracy [19], using these test parts represents a worst-case scenario. Therefore, we expect that the insights we gained from conducting experiments with our respective test parts allow us to draw conclusions that hold true for additional workpieces.

In addition to supporting the appearance of image artefacts, we extended the test parts with an insert that allows to calculate a resolution parameter (magnification in figure 3). By analyzing how the contact region between the spherical end of the insert and the touching plane of the test part is reconstructed, the resolution parameter can be determined (cf section 2.3.3).

2.2. Manufacture validation parts (figure 2, I.2)

In addition to the test parts, we designed validation parts (figure 5). We used these special workpieces to validate that results obtained from using the test parts are transferable to industrial workpieces. Therefore, the validation parts resemble typical industrial workpieces: (a) a plastic connector case, (b) a metal valve housing and (c) a metal cog wheel. Figure 5 shows a sketch of the validation parts that depicts the validation parts' measurement features.

While looking like industrial workpieces, the validation parts were specially designed for carrying out the validation of the CBR system. By using specifically designed validation parts instead of actual industrial workpieces, it was possible to manufacture the workpieces for validation in different sizes and materials which were previously not covered by the test parts:

(a) Validation case (val. Case) made from acrylonitrile butadiene styrene with 70 mm length,
(b) Validation housing (val. Housing) made from aluminum (AlMg4,5Mn0,7) with 40 mm length,
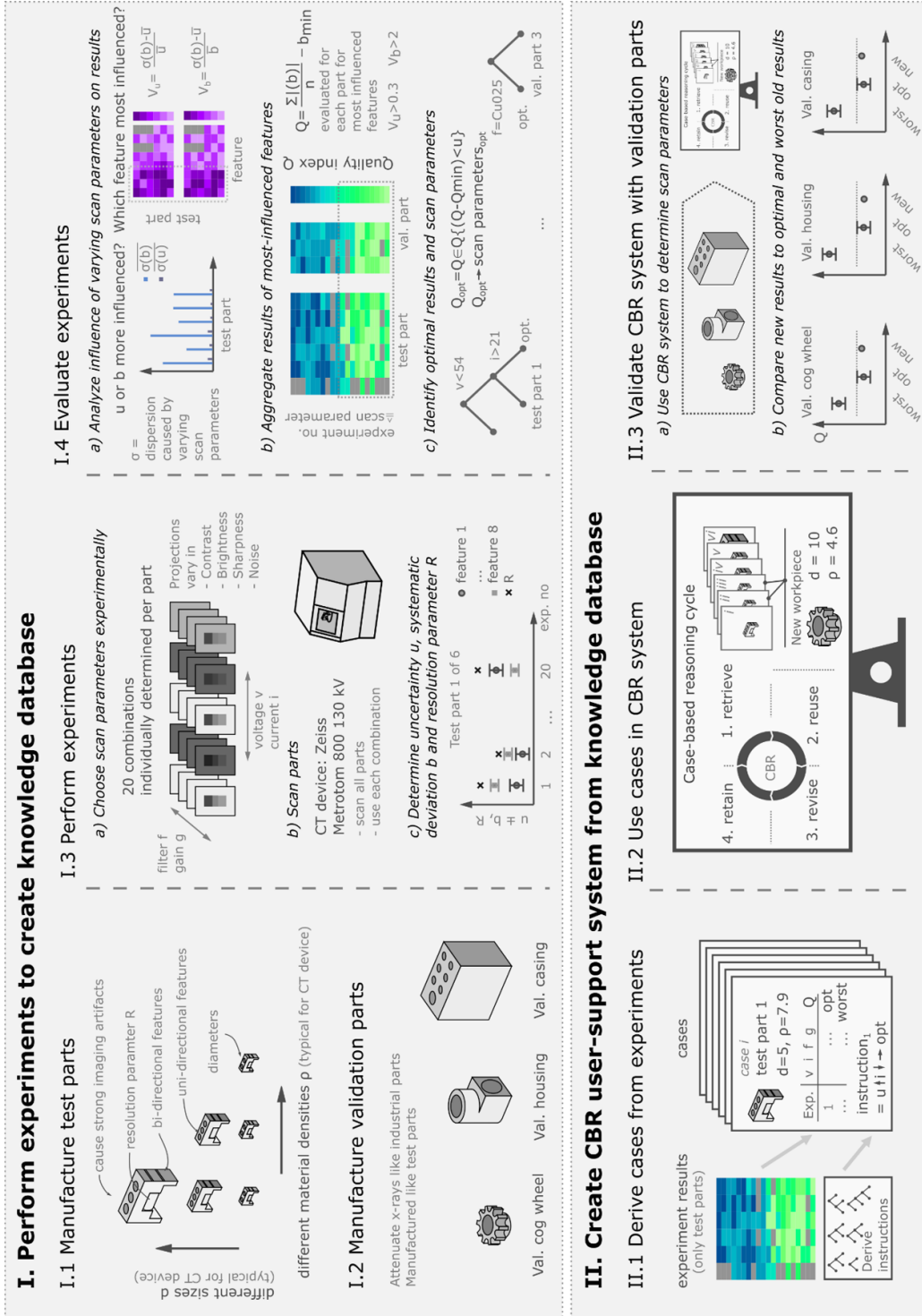(c) Validation cog wheel (val. Cog wheel) made from titanium (TiAl6V4) with 10 mm diameter.

Figure 2. Overview over this paper's structure.
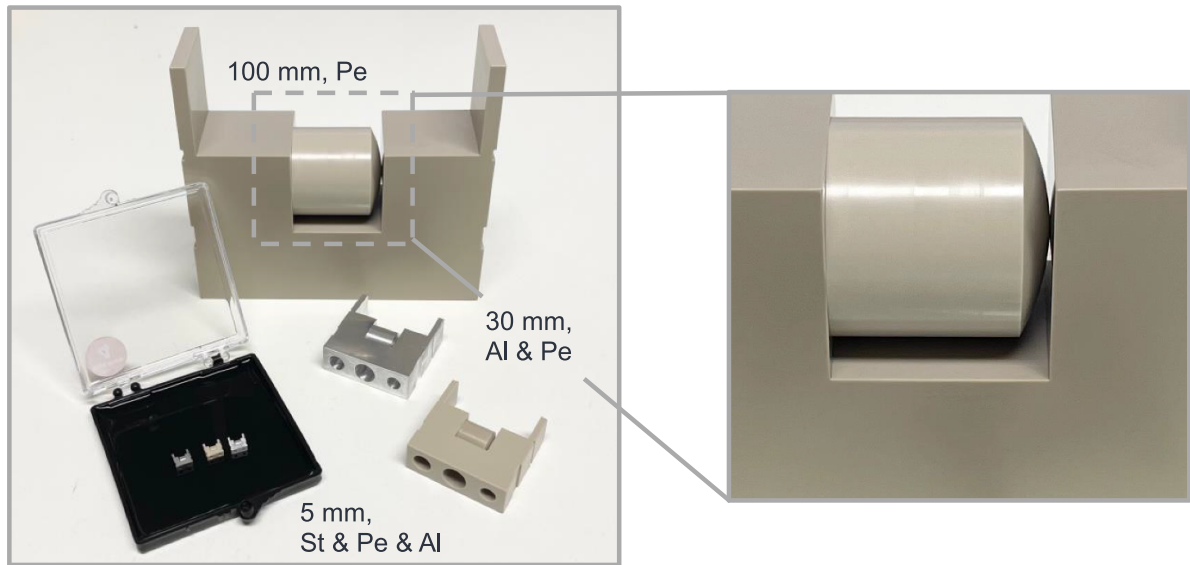
Figure 3. Photograph of the manufactured test parts and a magnified view of the insert used for calculating a resolution parameter.
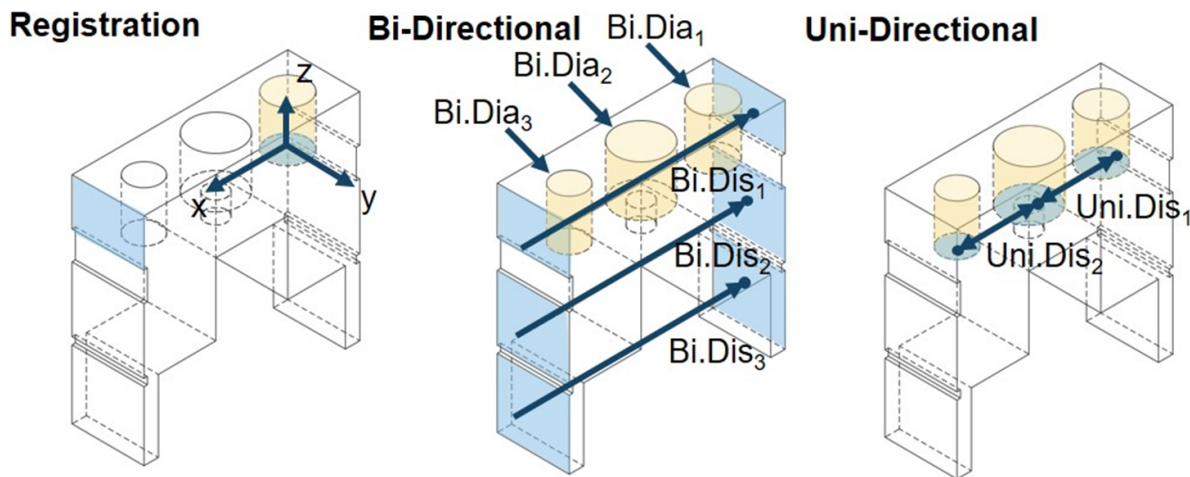
Figure 4. Test parts used for the experimental design and schematic visualization of their measurement features (insert not depicted).

Table 1. Nominal test part dimensions in mm.

Test part size	Bi-directional distances	Uni-directional distances	Diameters
5	5	2.6	0.9–1.1
30	30	10	4.5–7
100	100	34	18–22

Additionally, due to their carefully designed shape, we could manufacture the validation parts by high-precision milling. Compared to typical industrial manufacturing processes like injection molding or pressure casting, which would have normally been used in industrial production for such workpieces, using high-precision milling ensured low form errors, which allowed repeatable registration and low uncertainty reference measurements.

2.3. Perform experiments (figure 2, I.3)

After manufacturing the test parts, we used them to conduct experiments with varied scan parameters. We used a specific experimental design to analyze a potential connection between scan parameters and measurement results. The experimental design also aimed to strike a balance between covering most permissible combinations of scan parameters as well as limiting the total number of experiments.

Figure 5. Schematic visualization of the validation parts' measurement features.

a) Projections with different image appearance resulting from using five different v and i combinations

b) Respective five v- and i-combinations

Figure 6. Experimental approach to choose v- and i-levels for the experimental design by varying image appearance in respect to the detector's exposure limits W.

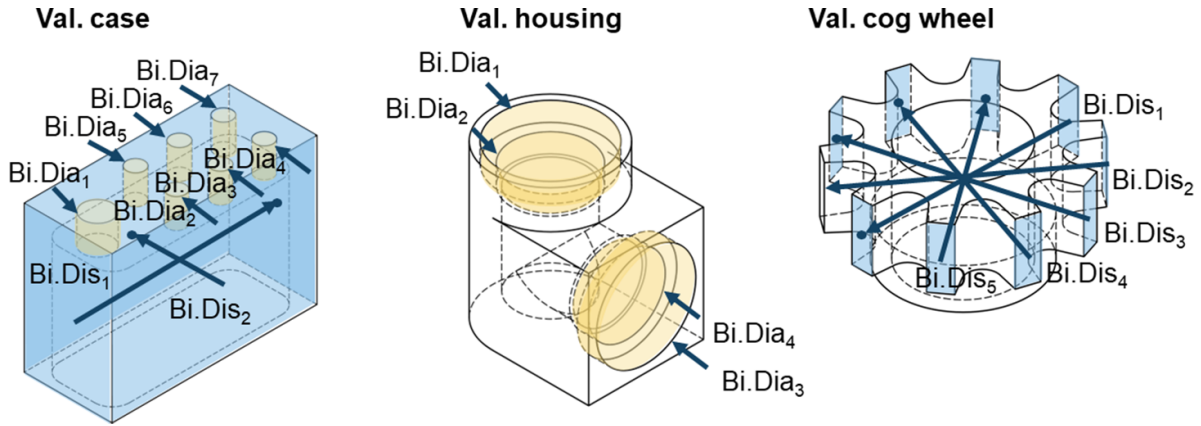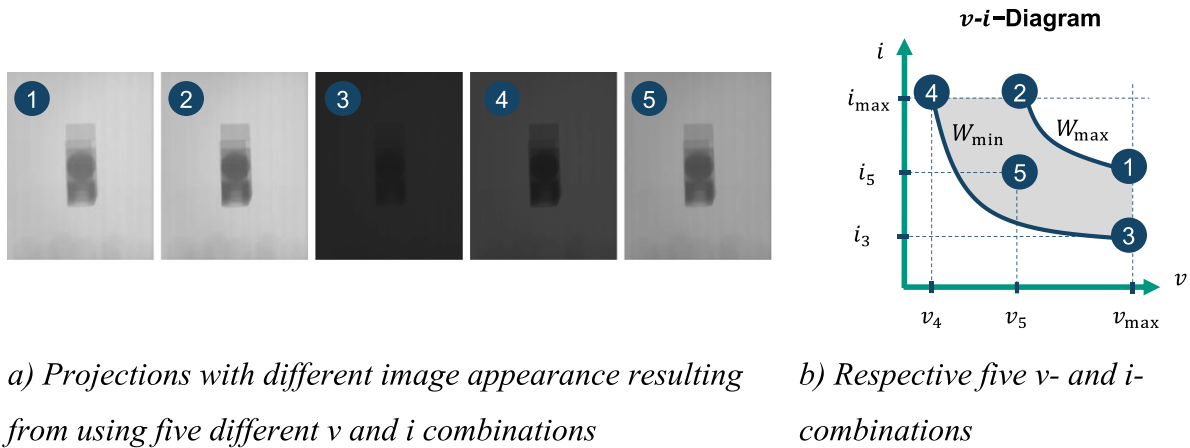For all measurements, we calculated the measurement uncertainty and systematic errors by using a specialized approach based on VDI/VDE 2630 2.1 [20]. Additionally, we determined the resolution parameter mentioned with an approach based on the work of Zanini and Carmignato [14].

2.3.1. Choose scan parameters experimentally. We chose the scan parameters for the experimental design experimentally. After placing the test parts in the CT device, we varied the x-ray source's current i, voltage v and filter f as well as the detector gain g to manipulate the projections' brightness, contrast, image noise and sharpness. To influence the projection' sharpness, we controlled the x-ray's power consumption $p = vi$ as we knew from the used CT device's technical specifications that the power consumption caused the focal spot's size to vary ($p < 8\,\text{W} \rightarrow 8\,\mu\text{m}$, $p < 16\,\text{W} \rightarrow 20\,\mu\text{m}$, $p > 16\,\text{W} \rightarrow 40\,\mu\text{m}$).

In total, we used 20 different scan parameter combinations C for every test and validation part. We used two different gain g and filter f levels which we experienced to be typical of the respective part. For each f–g-combination we chose five v–i-combinations. Figure 6(a) shows respective projections for a

given test part and f–g-combination to demonstrate the difference in image appearance.

Figure 6(b) schematically shows the five different v–i-combinations with respect to the detector's exposure limits (W_{max} and W_{min}) and the x-ray source's maximal v- and i-values ($v_{\text{max}} = 130\,\text{kV}$, $i_{\text{max}} = 300\,\mu\text{A}$). To obtain the first four combinations, we set $v = v_{\text{max}}$ or $i = i_{\text{max}}$ to their respective maximal values ($v_{\text{max}} \rightarrow 1, 3$, $i_{\text{max}} \rightarrow 2, 4$). Then we changed the respective other scan parameter ($v_{\text{max}} \rightarrow i$, $i_{\text{max}} \rightarrow v$) in order to just not over-expose (points 1 and 2) or under-expose (points 3 and 4) the projections.

In addition to these four corner points (1–4), we also used a central point 5. For point 5, we calculated the mean voltage $v_5 = (v_1 + v_4)/2$ of points 1 and 4 and set i in a way that resulted in a centered projection's histogram. That means that the average W_{mean} of the grey value-maxima in the projection's histogram of the workpiece's thickest region W_{part} and the background W_{back} equals the mean of the exposure limits W_{max} and W_{min} ($W_{\text{mean}} = (W_{\text{part}} + W_{\text{back}})/2 = (W_{\text{max}} + W_{\text{min}})/2$).

2.3.2. Scan parts. After determining the scan parameters, we chose magnification values by placing all parts in the rotation stage's center and moving the parts close to the

detector while ensuring that each projection still showed the whole, respective part. This resulted in the following voxel sizes: 5 mm test parts: 7 μm, 30 mm test parts: 39 μm, 100 mm test part: 130 μm, val. Cog wheel 14 μm, val. Housing 52 μm, val. Case 91 μm. We then scanned each part capturing 1500 projections with an exposure time of 1000 ms covering 360°. Using the CT device's software (Zeiss METROTOM OS 3.2), we performed reconstruction deploying the Feldkamp algorithm. To conduct the scans of the test parts and validation parts, we used the individually determined scan parameter combinations C from section 2.3.1. Thus, we conducted 20 scans for each of the six test parts and three validation parts (180 CT scans in total).

Additionally, we repeated CT scans for two scan parameter combinations C for every test part P. For these repetitions, we only considered combinations C_5 from point 5 in the v–i-diagram because they represent an average of the other four combinations C_1–C_4. From the four possible combinations C_5 (one for each f–g-combination), we chose those two combinations $C_{5,\mathrm{max}}$ and $C_{5,\mathrm{min}}$ that resulted in the highest and lowest contrast-to-noise ratio (CNR) of the reconstruction, respectively. We repeated the experiments for the highest CNR combination $C_{5,\mathrm{max}}$ five times including repositioning the part (i.e. removing it from the CT device between measurements) and another five times without repositioning. For the lowest CNR combination $C_{5,\mathrm{min}}$, we repeated experiments five times without repositioning.

2.3.3. Measurement uncertainty, systematic error and resolution parameter

2.3.3.1. Measurement uncertainty and systematic error.
To determine the measurement uncertainty and systematic error, we designed a procedure based on the guideline VDI/VDE 2630 2.1 [20]. We modified VDI/VDE 2630 2.1 to be evaluable with significantly less measurements, while still allowing to assess random and systematic effects. The determined systematic errors and expanded uncertainties will be called b and U, respectively.

In an initial step, we evaluated each experiment's reconstruction to obtain CT measurement results for all test parts and their features. We automated the evaluation with measurement templates and macros in VGStudio MAX. To determine the surface, we used a global surface determination process (VGStudio MAX standard setting). This surface determination process finds the two main phases' respective peaks in the reconstruction's histogram and determines the surface voxels' grey value as the mean of the grey values associated to the main phases' peaks.

In a second step, we calibrated all test parts using a tactile coordinate measuring machine (O-INSPECT 322 with Calypso 2018, both by Zeiss, Germany) and calibrated standards (gauge blocks and setting rings). We estimated the systematic error b according to equation (1) by subtracting the CT measurement values y_{CT} from the corresponding calibration values $\bar{y}_{\mathrm{cal}}$,

$$b = y_{\mathrm{CT}} - \bar{y}_{\mathrm{cal}}. \tag{1}$$

In the third and final step, we calculated the expanded measurement uncertainty U according to equation (2) by using a coverage factor $k = 2$ and evaluating the standard uncertainty of the measurement process u_{p} as well as the standard uncertainty of the calibration u_{cal}. We considered all other standard uncertainties described in VDI/VDE 2630 2.1 (u_{drift}, u_w and u_b) to be negligible as we conducted all measurements in a short time span (u_{drift}), used the same test parts for the calibration and the CT measurements (u_w) and conducted all measurements in the same measurement room at 20 °C (u_b),

$$U = k\sqrt{u_{\mathrm{cal}}^2 + u_{\mathrm{p}}^2}. \tag{2}$$

To calculate u_{p} according to equation (3), we used the results from the repeated measurements. We determined a standard uncertainty $u_{\mathrm{p},5,\mathrm{max}}$ for the results using combinations $C_{5,\mathrm{max}}$ with high CNR and repetitions including repositioning by calculating the standard deviation. To compensate for using less than 20 measurements, we multiplied $u_{\mathrm{p},5,\mathrm{max}}$ by a safety feature s derived from the t-distribution and the number of experiment repetitions as described by Schmitt *et al* and Müller *et al* [21, 22]. We accordingly calculated standard uncertainties $u_{\mathrm{rep},5,\mathrm{max}}$ and $u_{\mathrm{rep},5,\mathrm{min}}$ for the repetitions without repositioning for combinations $C_{5,\mathrm{max}}$ with high CNR and $C_{5,\mathrm{min}}$ for low CNR, respectively. By using the CNR of each experiment, we then estimated the standard uncertainty u_{p} for any given experiment based on its image quality CNR and the previously determined standard uncertainties. Utilizing this CNR-based estimation, we limited the number of experiments to 35 measurements per test part,

$$u_{\mathrm{p}} = u_{p,5,\mathrm{max}} + \frac{u_{\mathrm{rep},5,\mathrm{max}} - u_{\mathrm{rep},5,\mathrm{min}}}{\mathrm{CNR}_{5,\mathrm{max}} - \mathrm{CNR}_{5,\mathrm{min}}}\left(\mathrm{CNR}_{5,\mathrm{max}} - \mathrm{CNR}\right). \tag{3}$$

2.3.3.2. Resolution parameter.
In addition to determining the measurement uncertainty U and systematic errors b, we evaluated a resolution parameter (R). We based the approach to evaluate R on the two-spheres method presented by Zanini and Carmignato [23]. However, rather than using two touching spheres, we modified the approach to use a single insert with a spherical end that touches a flat wall (magnification in figure 3).

After surface determination, we fitted circles to the spherical end along the insert's axis and calculated the distance between circles from the touching plane in vertical direction. Figure 7 shows the distance of one circle taken as an example with respect to the touching plane. This distance is denoted by h_i and the attached radius by r_i. Additionally, we fitted a sphere to the top of the insert. The distance of the sphere center to the plane is denoted by a_{K}, and the sphere's radius by r_{K}. Subsequently, we calculated the reference height h_{ref} by equation (4),

$$h_{\mathrm{ref},i} = a_{\mathrm{K}} - \sqrt{r_{\mathrm{K}}^2 - r_i^2}. \tag{4}$$
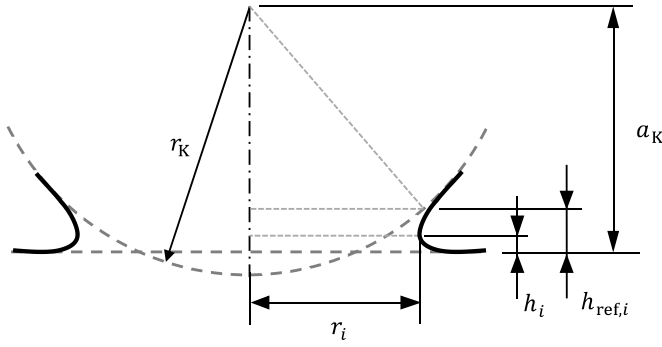
Figure 7. Sketch for calculating the resolution parameter *R*.

We calculated the difference between reference height $h_{\text{ref,i}}$ and circle height h_i. According to equation (5), we defined the lowest height h_i that led to a difference of less than 20% of $h_{\text{ref,i}}$ to be equal to the resolution parameter *R*,

$$R = \min_{h_i \in h} \left(\frac{h_{\text{ref,i}} - h_i}{h_{\text{ref,}i}} < 0.2 \right). \tag{5}$$

2.4. Evaluate experiments (figure 2, I.4)

Next, we evaluated the experiments. The evaluation's goal was to understand which scan parameters influenced the metrological values, and how to choose scan parameters to achieve optimal measurement results ('optimal measurement results' are defined in section 2.4.3).

2.4.1. Analyze the influence of varying scan parameters on results (figure 2, I.4 a).
To understand the influence of the scan parameters on the measurement results, we calculated the quality index (*Q*) that represents each experiment's accuracy. To calculate *Q*, we first investigated whether varying the scan parameters primarily influenced the systematic error *b* or the uncertainty *U*. Then, we checked which features were most influenced by varying the scan parameters. These most-influenced features were aggregated in a final step to calculate *Q*.

2.4.1.1. Investigating influence on systematic errors and uncertainty.
To investigate whether the scan parameters primarily influenced the systematic errors *b* or the uncertainty *U*, we determined the dispersion of the systematic errors *b* and uncertainty *U* caused by the different scan parameter combinations *C*, $\sigma(b)_{f,P}$ and $\sigma(U)_{f,P}$ for each feature *F* of each test part *P*. We quantified the dispersions $\sigma(b)_{f,P}$ and $\sigma(U)_{f,P}$ caused by using n_C different scan parameter combination *C* by calculating the respective standard deviations of all values of *b* and *U* of the same feature *F* of a given part *P* for all scan parameter combinations *C*. After calculating the dispersion $\sigma(b)_{f,P}$ and $\sigma(U)_{f,P}$ for each feature individually, we calculated the mean values of the dispersions, $\overline{\sigma(b)_P}$ and $\overline{\sigma(U)_P}$, for each test part *P*.

Comparing $\overline{\sigma(b)_P}$ and $\overline{\sigma(U)_P}$, we found that the mean dispersion of the systematic errors $\overline{\sigma(b)}$ was higher than the

dispersion of the uncertainty $\overline{\sigma(U)}$ for all test parts *P* figure 8. This means that varying the scan parameters mainly influenced the systematic error *b* and not the uncertainty *U*. Consequently, further evaluation steps focused on the systematic error *b*.

2.4.1.2. Identifying most-influenced features.
Next, we analyzed if some particular measurement features were more strongly influenced by varying the scan parameters than others. To identify these measurement features, we defined the uncertainty ratio V_U and the deviation error-ratio V_b according to equations (6) and (7) for each feature *F* of each test part *P*, respectively. These ratios allowed us to compare the mean uncertainty $\bar{U}$ and the mean systematic error $\bar{b}$ to the dispersion of the systematic error $\sigma(b)$ caused by using different scan parameter combinations *C* for the different experiments,

$$V_{U,F,P} = \frac{\sigma(b)_{f,P} - \bar{U}_{f,P}}{\bar{U}_{f,P}} \tag{6}$$

$$V_{b,F,P} = \frac{\sigma(b)_{f,P} - \bar{U}_{f,P}}{\bar{b}_{f,P}}. \tag{7}$$

The uncertainty ratio V_U and deviation ratio V_b of all test parts *P* are depicted in figures 9 and 10, respectively. In the figures, individual test parts *P* are reported on the vertical axis while measurement features *F* are displayed on the horizontal axis. Grey values indicate that a certain test part does not comprise the respective features (section 2.1 explains which parts comprise which features).

Figure 9 highlights that systematic errors *b* related to bi-directional distances $f_{\text{Bi.Dis}}$ show high values of the uncertainty ratio $V_U > 2$. This means that the systematic errors *b* of these features were strongly influenced by a variation of the scan parameters compared to the mean uncertainty $\bar{U}$ of these features. In other words, this indicates that the scan parameters mainly influenced results of bi-directional distances $f_{\text{Bi.Dis}}$.

A few other features showed high V_U values (100 mm Pe and 30 mm: Al Bi.Dia1 and Bi.Dia2, 30 mm Pe: Bi.Dia1, 5 mm Pe: Uni.Dis1), as well. However, these features only had a low deviation ratio $V_b < 0.3$, which means that the dispersion of these features' systematic errors $\sigma(b)$ caused by a variation of the scan parameters was small compared to the features' average systematic errors $\bar{b}$ (figure 10).

Therefore, only results related to bi-directional distances $f_{\text{Bi.Dis}}$ were further considered for the following investigations. 100 mm Pe Bi.Dis3 and 5 mm Pe Uni.Dis1 were treated as outliers in this context.

2.4.2. Aggregate results from most-influenced features to calculate quality index Q (figure 2, I.4 b)

2.4.2.1. Formulae for calculating quality index Q.
Next, we calculated the sum of absolute values of the systematic errors *b* for features f_V with values of $V_U > 2$ and $V_b > 0.3$ for each part *P* and scan parameter combination *C* to determine the average error *E* according to equation (8),
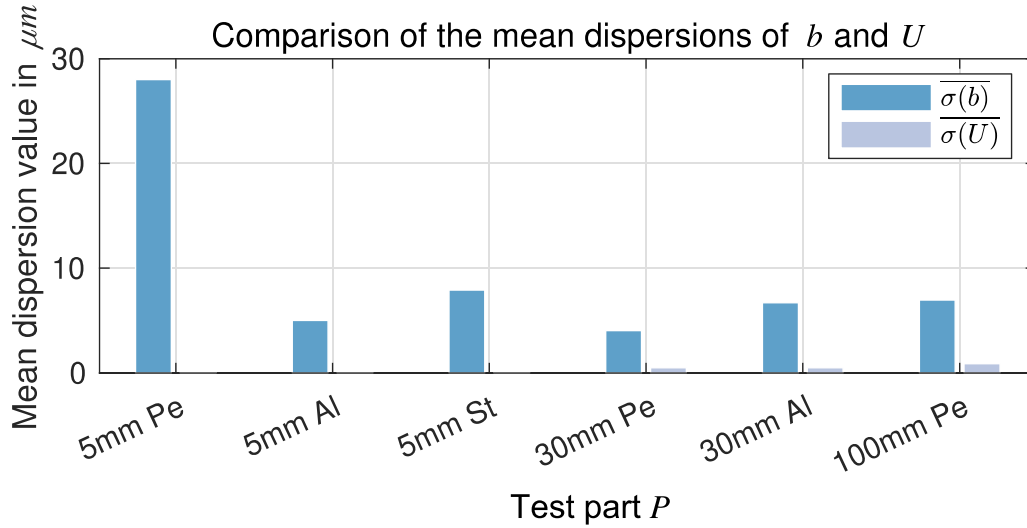
Figure 8. Comparison of mean dispersion values, $\overline{\sigma(b)}_P$ and $\overline{\sigma(U)}_P$, to analyze if b or U are influenced by the scan parameters.
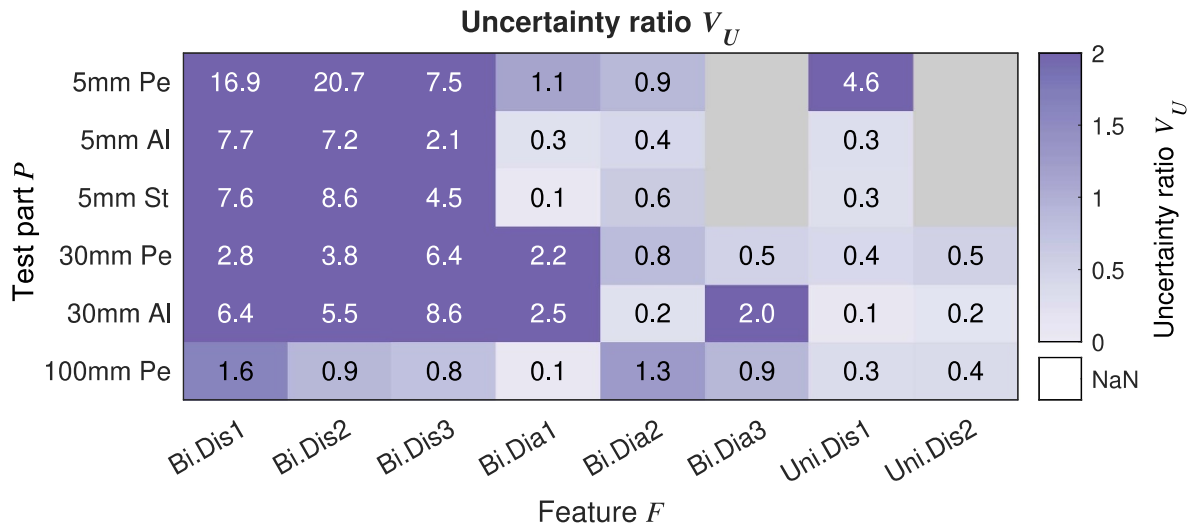

Figure 9. Uncertainty ratio V_U identifies features that showed significant dispersion of the systematic errors caused by varying scan parameters compared to the mean uncertainty.

$$E_{P,C} = \frac{\sum_{i=1}^{n_{F_V}} |b_{P,C,i}|}{n_{FV}}. \tag{8}$$

We then determined the quality index Q for each test part P and each scan parameter combination C by subtracting the smallest average error of the respective test part $E_{P,\min}$ from each value of the average error $E_{P,C}$, as shown in equation (9),

$$Q_{P,C} = E_{P,C} - E_{P,\min}. \tag{9}$$

The quality index Q only considers the results from those measurement features that can be actively influenced by the user's choice of scan parameters, making it ideally suited to

analyze the relationship between scan parameters and measurement results.

Additionally, regardless of which test part is analyzed, the best accuracy value is always $Q_{P,\min} = 0$, as this responds to the lowest average error $E_{P,\min}$ of the respective test part P. This allowed us to directly compare different test parts P in regards to the effect that varying the scan parameter combinations C had on the measurement results, as the best scan parameters led to a low value of the quality index $Q_{P,\text{best}} \approx 0$, regardless of which test part we investigated.

We individually decided for each validation part which measurement features to consider to calculate the quality index Q according to the following reasons.
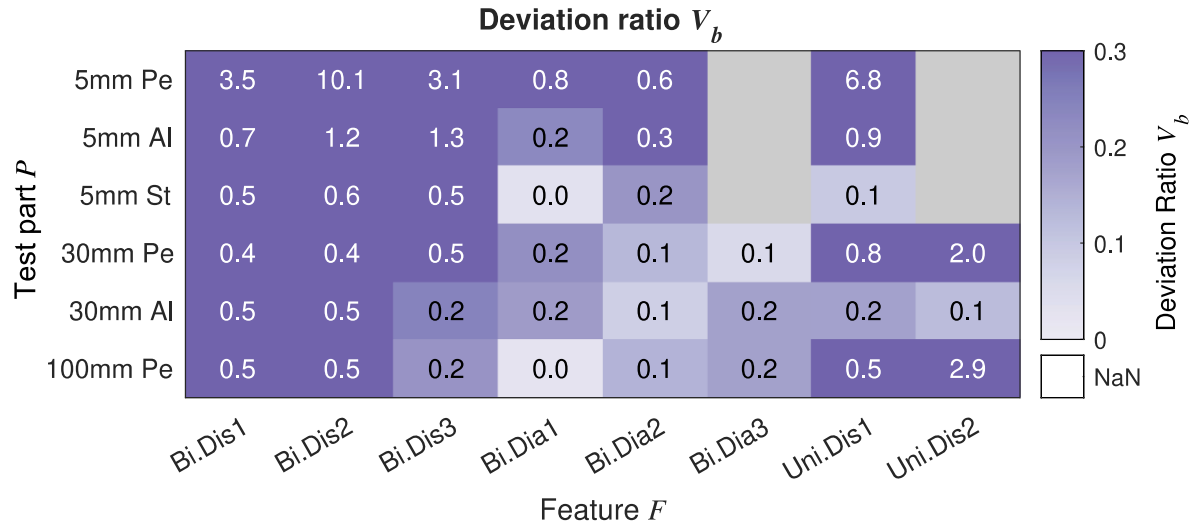
Deviation ratio V_b

Figure 10. Deviation ratio V_b identifies features that showed significant dispersion of the systematic errors caused by varying scan parameters compared to the mean systematic errors.

- Val. Cog wheel: Features related to the angles between the cog wheel's teeth showed large uncertainties of the calibration and were thus dismissed. As a consequence, we only calculated Q from the bi-directional distances between opposing teeth.
- Val. Housing: This validation part only comprises bi-directional diameters. We used the systematic errors b of these features to calculate Q.
- Val. Case: The systematic errors b of uni-directional distances between the holes on the top side as well their diameters were barley influenced by the scan parameters. Thus, we only used the bi-directional distances' systematic errors b to calculate Q.

2.4.2.2. Experimental results for quality index Q. Figure 11 shows the values of the average error E for all parts used in this study as box plots. Each boxplot contains the 20 E values from performing 20 experiments with each part P with varied scan parameters. The box plots' body and whisker sizes represent the dispersion of the average error E caused by using different scan parameters, while the box plots' position highlights the magnitude of systematic errors b identified for a specific test part.

The diagram highlights that the dispersion and the magnitude of the average error E increase with test parts size and material density. The test parts of higher material density and larger size led to higher systematic errors. The validation parts, however, were less influenced by a variation of the scan parameters. Of note, they did show similarly high median systematic errors compared to the test parts.

Figure 12 shows the quality index Q. Different scan parameter combinations C are arranged above the vertical axis while test parts P and validation parts are displayed along the

horizontal axis. Scan parameter combinations C are given in a coded form: the first number refers to the combination of filter f and gain g, and the second number refers to the specific point in the v–i-diagram shown in figure 6. Concerning the first number, number 1 refers to a thin filter f_- and a low gain level g_-, 2 to a thin filter f_- and high gain level g_+, 3 to a thick filter f_+ and a low gain level g_-, and 4 to a thick filter f_+ and a high gain level g_+. For example, 2_4 means that a particular experiment was carried out with a thin filter f_- and high gain level g_+ and a v–i-combination from point 4, which maximizes i_+ while minimizing v_-.

Figure 12 shows that combinations C in the lower half of the diagram (3_x, 4_x) caused smaller systematic errors b. This means scan parameters with a thick filter (f_+) ensured low Q values, i.e. small errors. Additionally, for a given combination of filter f and gain g, combinations C that belong to point 3 in the v–i-diagram caused smaller Q values for 5 mm test parts made from metal (aluminum and steel). Point 3 refers to high voltage v_+ and low current i_-. Such combinations limit the x-ray source's power consumption for a given level of detector exposure W. An in-depth interpretation will be provided together with an analysis of the resolution parameter R below. The validation parts showed lower maximal errors in the upper part of the heatmap than test parts 5 mm St, 30 mm Al and 100 mm Pe. They seemed to be less sensitive to the scan parameter choice.

According to equation (9), the smallest value of the quality index Q for each test part P is 0. For a given part, this value corresponds to the smallest value of the average error $E_{P,\min}$ represented by the lowest part of the lower whisker of each box plot in figure 11. With respect to this, the average error E boxplots (figure 11) are well suited to compare the magnitude of error, while the quality index Q heatmap (figure 12) shows the results from varying the scan parameters combinations C. Together, the boxplots and the heatmap allow us to understand
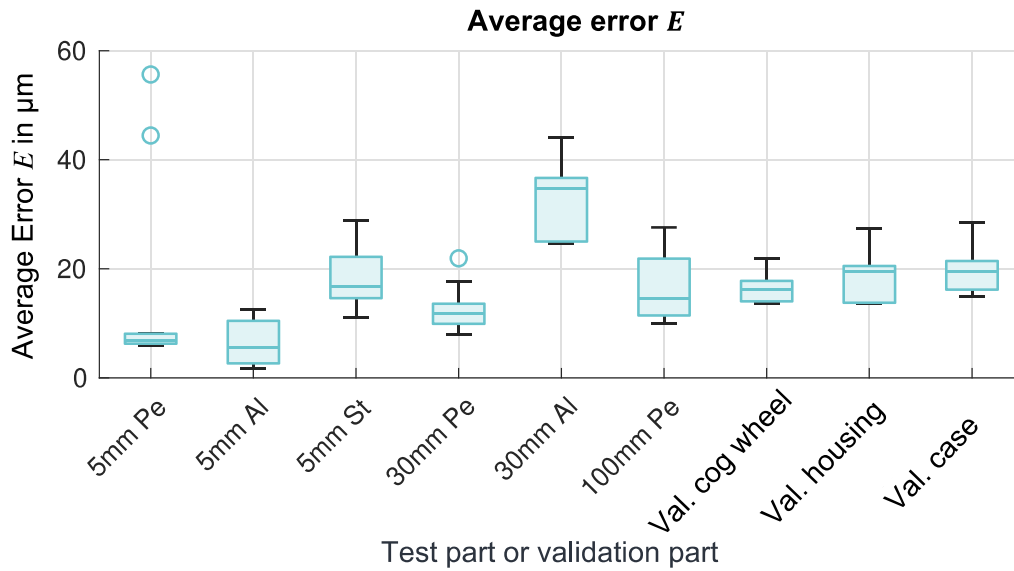
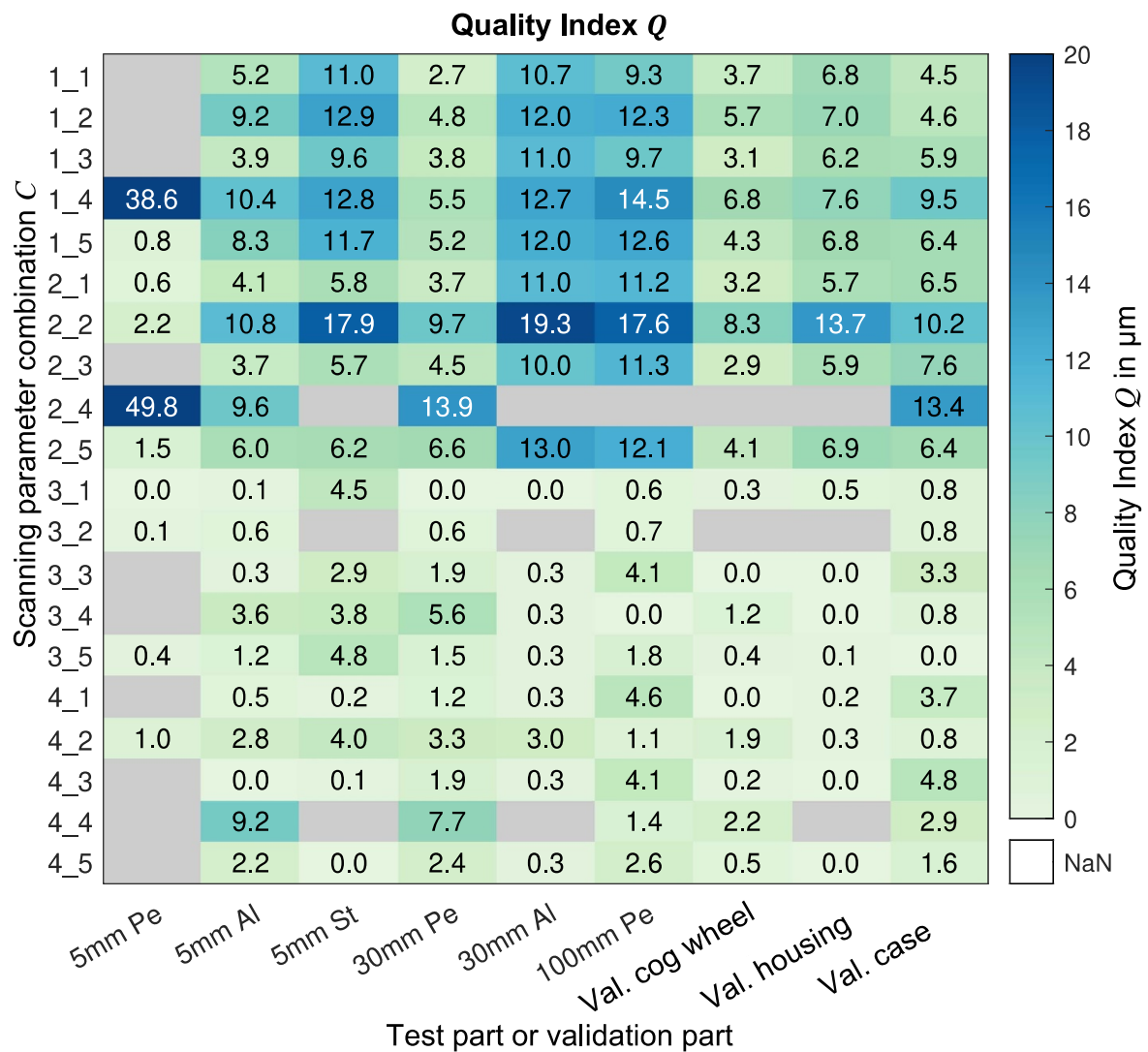**Figure 11.** Box plots of average errors E to compare test parts P.

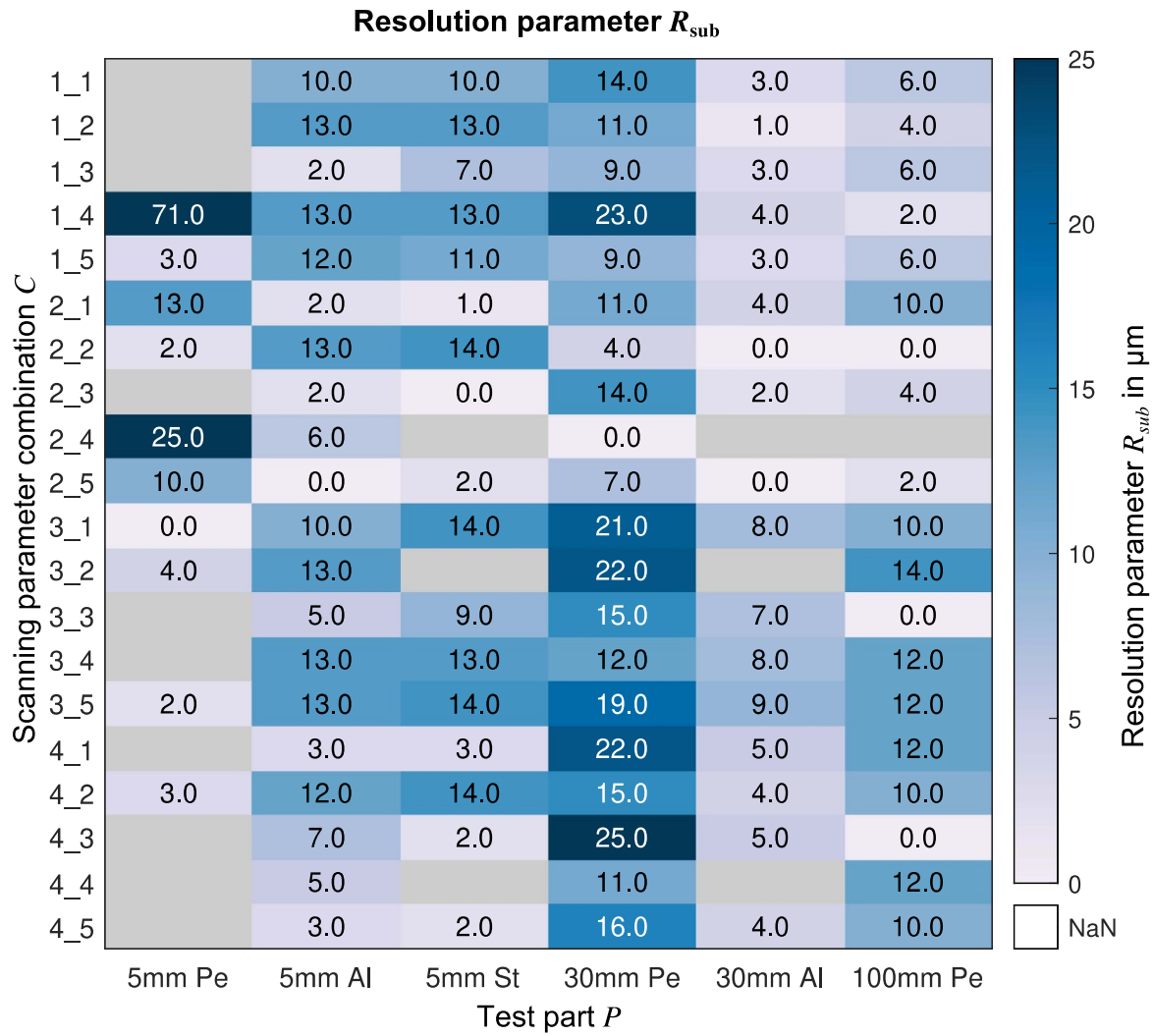**Figure 12.** Quality index Q heatmap to compare scan parameter combinations C of different test parts P.

Resolution parameter R_{sub}

Scanning parameter combination C	5mm Pe	5mm Al	5mm St	30mm Pe	30mm Al	100mm Pe
1_1		10.0	10.0	14.0	3.0	6.0
1_2		13.0	13.0	11.0	1.0	4.0
1_3		2.0	7.0	9.0	3.0	6.0
1_4	71.0	13.0	13.0	23.0	4.0	2.0
1_5	3.0	12.0	11.0	9.0	3.0	6.0
2_1	13.0	2.0	1.0	11.0	4.0	10.0
2_2	2.0	13.0	14.0	4.0	0.0	0.0
2_3		2.0	0.0	14.0	2.0	4.0
2_4	25.0	6.0		0.0		
2_5	10.0	0.0	2.0	7.0	0.0	2.0
3_1	0.0	10.0	14.0	21.0	8.0	10.0
3_2	4.0	13.0		22.0		14.0
3_3		5.0	9.0	15.0	7.0	0.0
3_4		13.0	13.0	12.0	8.0	12.0
3_5	2.0	13.0	14.0	19.0	9.0	12.0
4_1		3.0	3.0	22.0	5.0	12.0
4_2	3.0	12.0	14.0	15.0	4.0	10.0
4_3		7.0	2.0	25.0	5.0	0.0
4_4		5.0		11.0		12.0
4_5		3.0	2.0	16.0	4.0	10.0

Test part P — Resolution parameter R_{sub} in µm (color scale 0–25, NaN)

Figure 13. Subtracted resolution parameter R_{sub} heatmap to compare scan parameter combinations C of different test parts P.

the influence of the test part properties and the scan parameters on the measurement accuracy.

2.4.2.3. In-depth interpretation from evaluating the resolution parameter R.

To allow further in-depth interpretation, we additionally considered the resolution parameter R. In resemblance of the quality index's equation (9), the lowest value $R_{\text{P, min}}$ achieved for each respective test part P was subtracted from each resolution parameter $R_{P,C}$ value to calculate the subtracted resolution parameter R_{sub} according to equation (10). This allowed us to compare scan parameter combinations C of different test parts P,

$$R_{P,C} = R_{P,C} - R_{P,\text{min}}. \tag{10}$$

Figure 13 depicts the subtracted resolution parameter R_{sub} for all scan parameter combinations C. The depicted heatmap's layout resembles the quality index's heatmap (vertical axis—scan parameter combination, horizontal axis—test part). The validation parts are not indicated in the diagram as they do not

comprise an insert that is necessary to calculate the resolution parameter R.

Evaluating the resolution parameter R_{sub} shows that parts made from plastic showed large differences for different scan parameter combinations. This could be attributed to the lower contrast values compared to metal parts that hampered the resolution parameter's accurate determination. Further details will be discussed in section 4.2.

Thirty millimeter Al showed small differences when varying the scan parameters. However, for 5 mm Al and 5 mm St, scan parameter combinations that led to low R values also showed good, i.e. low, Q values compared to the other scan parameter combinations that used similar filter and gain values (scan parameter combinations $C = $ 1_3, 2_1, 2_3, 2_5, 3_3, 4_1, 4_3, 4_5). Scan parameter combination 4_4 is treated as an outlier as this scan parameter combination led to very dark projections which in turn led to a very low CNR level. Not considering this outlier, the presented results allowed us to draw the conclusion that the measurements' resolution needs to be
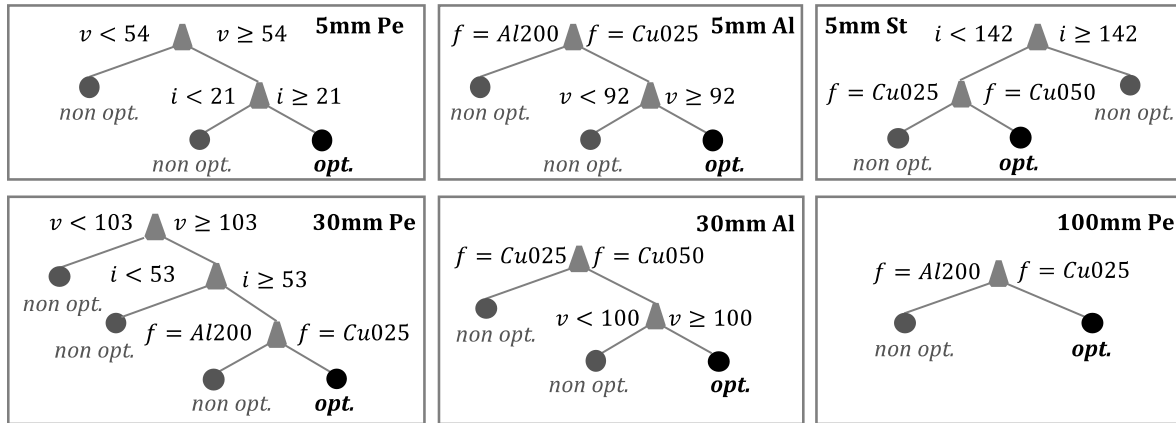
Figure 14. Decision trees to predict scan parameters (f, g, v, i) resulting in optimal measurement results (voltages in kV, current in μA and filter as shorthand in which thickness is referred to in 0.01 mm).

considered when aiming to achieve accurate measurements for small parts made form metal.

The above-mentioned scan parameter combinations all resulted in low power consumption of the x-ray source. In case of the used CT device, the x-ray source's power consumption directly affects the focal spot's size (as mentioned in section 2.3.1). Therefore, we assume that limiting the power by choosing scan parameters accordingly limits the focal spot size. This allows to achieve a high resolution and, consequentially, low errors.

2.4.3. Identify optimal results and scan parameters (figure 2, 1.4c). After evaluating the experiments' accuracy by calculating the quality index Q, we derived decision trees from the results to understand which scan parameters resulted in the best results.

2.4.3.1. Identify optimal results. In a first step, we determined so-called 'optimal results'. For this evaluation, we calculated the mean uncertainty $\bar{U}_{P,C}$ for each experiment as the mean value of all values of $U_{P,C,\text{Bi.dis}}$ belonging to bidirectional distance features. If an experiment's $Q_{P,C}$ value was lower than $\bar{U}_{P,C}$, we called its scan parameters combination $C_{P,\text{opt}}$ optimal (compare equation (11)),

$$Q_{P,\text{opt}} = Q_P \in Q_P\{(Q_{P,C} - Q_{P,C,\text{min}}) < \bar{U}_{P,C}\}. \quad (11)$$

By finding all optimal combinations $C_{P,\text{opt}}$ for each test part P, we identified scan parameters $(f, g, v, i)_{P,\text{opt}}$ associated with optimal results $Q_{P,\text{opt}}$.

2.4.3.2. Find similarities of optimal scan parameters. In a second step, we trained decision tree models T_P to predict optimal results $Q_{M,P,\text{opt}}$ from optimal scan parameters $(f, g, v, i)_{P,\text{opt}}$ for each part P (compare equation (12)),

$$T_P(f, g, v, i) = Q_{P,\text{opt}}. \quad (12)$$

Figure 14 shows the test parts' trained decision trees T_P. We use qualitative assessment (indicated by subscripts $+$ and $-$)

for the following interpretation while quantitative values are given in figure 14.

For small parts made from metal (5 mm Al, 5 mm St), a thick filter f_+ and a high voltage v_+ or low current i_- led to optimal results. This can be explained by such v–i combinations' low power consumption of the x-ray source. This is due to detector exposure W being proportional to $W \sim u^2 i$ [24]. Therefore, scan parameters with high voltage v_+ or low current i_- ensure lowest power consumption for a given detector exposure W. As previously mentioned, limited power leads to a high resolution and, in turn, good quality index Q values for small parts made from metal. In case of the 30 mm Al test part, a high voltage v_+ and a thick filter f_+ were necessary to achieve optimal results. In summary, high voltages v_+ and thick filters f_+ led to optimal results for metal parts (5 mm St, 5 mm Al, 30 mm Al).

Test parts made from Pe showed a different behavior. The 5 mm and 30 mm Pe parts demanded both a high voltage v_+ and high current i_+. Additionally, 30 mm Pe required a thick filter f_+. While 100 mm Pe did not demand for high voltage v_+ and current i_+ values, it did require a thick filter f_+ to achieve optimal results. In general, high power p_+ and thick filters f_+ led to optimal results for plastic parts.

These findings resulted in two generalized rules:

(a) Small parts made from metal needed to be scanned using thick filters f_+. Further, a high voltage u_+ allowed to limit the current i and thus power consumption to ensure a small focal spot size.
(b) Large metal parts and parts made from plastic needed to be scanned with a thick filter f_+ and both a high voltage v_+ and high current i_+.

The first rule helps to limit beam hardening artifacts by deploying a thick filter. It also ensures a small focal spot size through limiting the x-ray source's power consumption. The small focal spot leads to high image sharpness and high resolution. The second rule also relies on using a thick filter to limit beam hardening. Additionally, the projections' brightness is
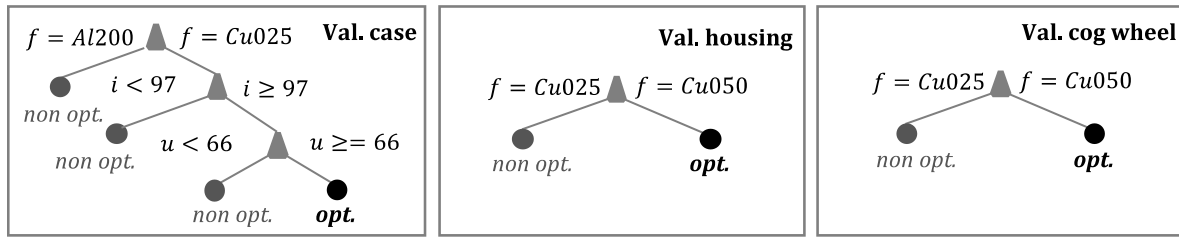
Figure 15. Decision trees to predict scan parameters (f, g, v, i) to obtain optimal measurements for the validation parts (voltages in kV, current in µA and filter as shorthand in which thickness is referred to in 1/100 mm).

increased by maximizing voltage and current. This boosts the CNR of a reconstruction.

The tree rules of the validation parts depicted in figure 15 showed a slightly different behavior. In comparison to the test parts, they were not as strongly affected by the choice of the scan parameters. Nevertheless, the above presented generalized rules from the test parts were still valid to achieve optimal results for the validation parts.

3. Create CBR user-support system from knowledge database (figure 2, II)

3.1. Derive cases from experiments (figure 2, II.1)

To create the CBR user-support system, we started by deriving cases from the experiments.

We decided to identify different cases by the respective workpieces' size d and material density ρ. While there are many characteristics that define a workpiece's individual properties, these two proved to be sufficient for this work. The discussion in section 4 explains how to include further attributes and how including further attributes could help to handle more complicated CT systems.

By identifying cases by workpiece size d and density ρ, we combined all results belonging to a single test part P into one case. As a consequence, a case followingly comprised the scan parameters (f, g, u, i), the average error E and quality index Q. Thus, we derived six initial cases from the test parts' experiments (note: none of the validation parts' experiments were used to derive the initial cases).

To ensure that the CBR system is able to choose optimal scan parameters for previously unknown parts, we decided to include the in-depth understanding of the used CT device gained from interpreting the decision trees in section 2.4.3 into the initial cases. We did this by concretizing the two generalized rules derived from the trees as two sets of instructions I on how to fine-tune scan parameters.

As with the generalized rules, the first instruction I_1 was attributed to the 5 mm Al and 5 mm St parts, while the second instruction I_2 was attributed to the other parts.

(a) To achieve good results according to the first instruction I_1, …
  1. A matched case's thickest filter f_+, highest gain level g_+ and highest voltage v_+ must be used and

  2. then the current i must be set in respect to the voxel size Vx, in order to limit power to $p = 8$ W if $Vx < 16$ µm, to $p = 16$ W if $Vx > 16$ µm or that the darkest part W_{part} of the projections is close to but not underexposed.
(b) To achieve good results according to the second instruction I_2, …
  1. The matched case's thickest filter f_+, lowest gain level g_- and highest voltage v_+ must be used and
  2. then the current i must be set to either reach the maximum permissible current $i_{\max}$ or to expose the projection's brightest part W_{back} to be close to but not being overexposed.

3.2. Use cases in CBR system (figure 2, II.2)

After defining the initial cases, we set up the CBR user support system by implementing the CBR cycle as a MATLAB-based software tool.

3.2.1. Retrieve cases. To retrieve cases from existing cases, the user must provide the system with a new workpiece's material density ρ_{new} and maximal penetration length d_{new}. Our experiments showed that rough estimates of these attributes gained from technical drawings were sufficient to successfully retrieve matching cases.

The system identifies the suitable cases by calculating the similarity index λ from comparing the material density ρ_{new} and maximal penetration length d_{new} of a new workpiece to the material density ρ_{old} and maximal penetration length d_{old} of existing cases according to equation (13),

$$\lambda = \left(1 + 100\frac{|\rho_{\text{new}} - \rho_{\text{old}}|}{\rho_{\text{old}}}\right) + (1 + |(d_{\text{old}} - d_{\text{new}})|). \quad (13)$$

The CBR system identifies a case matching to the new workpiece by the lowest λ value. To identify representative cases, equation (13) balances penetration length and material density to judge the degree of similarity between a new workpiece and the existing cases.

3.2.2. Reuse cases. After matching a suitable initial case to a new workpiece, the CBR system uses knowledge stored in its cases to support a user to identify suitable scan parameters to successfully scan the new workpiece.

Before the CBR system recommends scan parameters, the user has to mount the workpiece in the CT device with an inclination angle of about $15°$. Next, the user must position the workpiece as close to the x-ray source as possible while still ensuring that the workpiece is fully visible in all projections. Finally, the user must set integration time $t = 1000\,\text{ms}$, number of projections $n = 1500$ ($360°$ rotation), no binning and Feldkamp algorithmn for reconstruction. We expect a user of the CBR system to have at least a basic level of training and therefore to know how to set these parameters. Note that the CBR system currently only supports setting these scan parameters (f, g, u, v). Other important parameters, like the number of projections n are discussed in section 4.

After confirming with the CBR system that initial setup has been finished, the user starts the CBR system's actual scan parameter choosing support process.

(a) The CBR system provides the user with the respective scan parameters $(f, g, u, v)_{\text{old,opt}}$ that led to optimal measurements $Q_{\text{old,opt}} = 0$ when measuring the matched case's workpiece.
(b) The CBR system provides the user with the matched case's set of instruction I_{old}.
(c) The CBR system prompts the user
　　1. to set the scan parameters $(f, g, u, v)_{\text{old,opt}}$ and
　　2. to fine-tune them using the instruction I_{old} to obtain new, CBR system-supported scan parameters $(f, g, u, v)_{\text{new}}$.
(d) Finally, the CBR system instructs the user to start the scan with the new, CBR system-supported scan parameters.

3.2.3. Revise cases.
To revise whether the CBR system's recommendations have led to satisfactory results, the user must conduct two additional, so-called revision measurements with the new workpiece. For these measurements, the CBR system provides those scan parameters $(f, g, u, v)_{\text{old},+}$ and $(f, g, u, v)_{\text{old},-}$ from the matched case that led to the best results $Q_{\text{old,min}} = Q_{\text{old},+}$ and worst results $Q_{\text{old,max}} = Q_{\text{old},-}$, respectively.

To evaluate the newly conducted experiments, the user must carry out the evaluation process according to section 2.4 (including measurement repetitions) to calculate the average error E and uncertainty U. The user must use the results $Q_{\text{old},+} = 0$ obtained with the scan parameters $(f, g, u, v)_{\text{old},+}$ to calculate $Q_{\text{old},+}$, $Q_{\text{old},-}$ and Q_{new}.

After evaluating them, the user must provide the values of the quality index Q and uncertainty U to the CBR system. Using $\bar{U}_{\text{new}}$, the CBR system decides whether the supported results Q_{new} were meaningfully different compared to the results from the previously best scan parameters $Q_{\text{old},+}$ by using equation (14),

$$|Q_{\text{old},+} - Q_{\text{new}}| < \bar{U}_{\text{new}}. \qquad (14)$$

Table 2. Results for the similarity index λ. Bold printing indicates which test parts were matched to the respective validation parts.

Test part	Val. cog wheel	Val. housing	Val. case
5 mm Pe	1483	3913	1589
5 mm Al	406	36	4222
5 mm St	**264**	2406	5831
30 mm Pe	5190	1196	987
30 mm Al	1421	**11**	2622
100 mm Pe	22491	6630	**746**

The CBR system calls the supported scan parameters $(f, g, u, v)_{\text{new}}$ satisfactory if the difference between the new results Q_{new} and the results using the previously best scan parameters $Q_{\text{old},+}$ is smaller than the average uncertainty $\bar{U}_{\text{new}}$.

The results using the previously worst scan parameters Q_{-} allow the user to decide if the advantage gained through the CBR system's support is meaningful.

The presented approach to revise a case is based on the evaluation process from section 2.4 and therefore causes substantial additional effort. However, this step is independent from reusing the old cases in the previous step, during which the CBR system provides the user with new scan parameters. The user can therefore decide whether revising the results is worth the additional effort. The discussion (section 4) provides an outlook on an image-quality-based analysis which could be included in future iterations of the CBR system to substantially reduce the revision's effort.

3.2.4. Retain cases.
After the new case's revision, the CBR system retains the new workpiece's attributes, the provided scan parameters and the revision' results (scan parameters and evaluation) by creating a new case. The CBR system saves the instruction from the matched case to the new cases, as well. For example, if the CBR system matched a new workpiece to the old case '5 mm St' the instruction from '5 mm St test' is transferred to the new workpiece's case.

3.3. Validate CBR system with validation parts (figure 2, II.3)

To validate if the CBR system is able to aid with choosing scan parameters that allow to achieve highly accurate results, the CBR system was tested with a CT user. For these tests, the user measured the validation parts with the CBR system providing support. We chose a student that worked as a research assistant at our department as the test user.

To **retrieve** the cases (section 3.2.1), the user provided the validation parts' material densities and penetration lengths to the CBR system which accordingly calculated the similarity index λ with equation (12). Table 2 shows the results. Based on these results, the CBR system matched

- val. cog wheel ($d = 10\,\text{mm}$, $\rho = 4.5\,\text{g mm}^{-3}$) to 5 mm St,
- val. housing ($d = 40\,\text{mm}$, $\rho = 2.7\,\text{g mm}^{-3}$) to 30 mm Al and
- val. case ($d = 70\,\text{mm}$, $\rho = 1\,\text{g mm}^{-3}$) to 100 mm Pe.

Table 3. Scan parameter combinations and results for the validation experiments.

Validation part	Scan para. combination	Filter	Gain	Voltage in kV	Current in μA	Q in mm	$\overline{U}$ in mm	Opt.
Val. cog	C_-	0.25 mm Cu	8.0×	76	300	0.006	0.003	No
wheel	C_+	0.5 mm Cu	2.5×	130	90	0.000	0.003	Yes
	C_{new}	0.5 mm Cu	8.0×	130	61	0.001	0.003	Yes
Val.	C_-	0.25 mm Cu	8.0×	76	300	0.014	0.001	No
housing	C_+	0.5 mm Cu	2.5×	130	180	0.000	0.001	Yes
	C_{new}	0.5 mm Cu	2.5×	130	202	0.000	0.001	Yes
Val. case	C_-	0.2 mm Al	8.0×	49	300	0.008	0.003	No
	C_+	0.25 mm Cu	2.5×	110	300	0.000	0.003	Yes
	C_{new}	0.25 mm Cu	2.5	130	202	0.001	0.003	Yes

To **reuse** the cases (section 3.2.2), the CBR system provided the user with the scan parameters $(f, g, u, i)_{\text{opt}}$ from the matching case that led to the best quality index Q_{opt} as well as the respective set of instructions I to modify the scan parameters.

For example, for val. cog wheel, the CBR system provided the thickest filter $f = 0,5\,\text{mm}\,\text{Cu}$, highest gain $g = 8.0x$ and highest voltage $v = 130\,\text{kV}$ from the matching case (5 mm St). Based on the set of instructions, the CBR system then prompted the user to increase current i until a power consumption $p = 8\,\text{W}$ was reached, while checking that the projection was not underexposed. The user accordingly chose $i = 8\,W/130\,kV = 61\,\mu A$. Table 3 shows the scan parameters combination C_{new} that the user determined with the CBR system's help to conduct val. cog wheel's (and the other validation parts') measurements.

To **revise** cases (section 3.2.3), the CBR system provided the user with the scan parameters $(f, g, u, v)_{\text{old},+}$ and $(f, g, u, v)_{\text{old},-}$ from the matched cases that led to the best results $Q_{\text{old,min}} = Q_{\text{old},+}$ and worst results $Q_{\text{old,max}} = Q_{\text{old},-}$, and instructed the user to conduct measurements with these. As we had already conducted measurements with the validation parts in sections 2.3 and 2.4 and therefore knew which scan parameters led to optimal and worst results respectively, we instructed the user to use these previously determined scan parameters. We also provided $\overline{U}$ values from the previous measurements.

After conducting the scans accordingly, we helped the user to evaluate the measurements as described in sections 2.3 and 2.4. Using the uncertainty according to equation (14), the CBR system decided whether it had provided scan parameters that resulted in optimal measurement results, i.e. results that are indistinguishable from the previously best results. The evaluated results in table 3 show that all CBR system-supported scan parameters led to optimal results. This also means that the CBR system was successful at helping the user to conduct accurate measurements of the validation parts.

To **retain** the cases (3.2.4), the CBR system prompted the user to enter the scan parameters the user had used for the measurement and saved them as additional new cases in the database.

4. Summary, discussion and outlook

4.1. Summary and key findings

Our approach consisted of two steps: first we performed experiments to create a knowledge data base (section 2, figure 2, I) and then we created a CBR user support system from the knowledge database (section 3, figure 2, II). The validation experiments showed that our approach was successful.

The foundation to this success was to deploy six different test parts made from different materials in different sizes and to measure each with systematically varied scan parameters that led to CT reconstructions with distinctly different image properties. By evaluating the respective results we gained detailed insights into the relationship between scan parameters, workpiece properties and accuracy of dimensional measurements.

In this context, it proved to be effective to design the test parts to evoke pronounced imaging artifacts like beam hardening. As a consequence, varying the scan parameters resulted in differentially pronounced image artifacts in the test parts' reconstructions and thus considerably different measurement results. Of note, the validation parts with their industrial workpiece-like shape were less sensitive to the choice of scan parameters. As a result, performing experiments with the test parts allowed us to create a knowledge database that empowered the CBR system to advise the user to choose sensible scan parameters. This enabled the user to perform accurate measurements of the validation parts, even though the validation parts had been previously unknown to the CBR system.

Using CBR to create a CT user support system proved to be more complex than expected because the experimental results had to be thoroughly evaluated by an expert to be usable in CBR cases. Revising the results of the CBR system in the third step of the CBR cycle also demanded for extensive expert's knowledge. Nevertheless, CBR proved to be well-suited to provide a non-expert user with pre-processed expert's knowledge gained from experiments.

Compared to other CT user support system approaches, e.g. using ray-tracing simulations [8, 9] or projection-based simulations [11], we considered workpiece properties as

factors in our experimental design. The result of the average error E (figure 11) shows that the workpiece properties have a large impact on the measurement deviation and thus accuracy. While the other approaches cover workpiece related factors by their underlying physical models [8, 9], our approach relies on covering all typically investigated workpieces by deploying test parts with accordingly chosen sizes and materials. Moreover, we were able to provide validation experiments with our industrial-like validation parts and thus showed that our experimental approach may lead to satisfactory results, while the other approaches lack a validation using different, industrial workpiece.

Additionally, our work differs from other comparable approaches as we designed our test and validation parts to be manufacturable in different sizes and materials. By choosing appropriate materials and sizes, our parts may be adopted for use with other CT systems or user support systems. This would, for example, allow to deploy the test parts to parameterize a simulation model. Then, measurements of the validation parts could be simulated to prove that the parameterized simulation model leads to a correct prediction of measurement results for previously unknown workpieces.

4.2. Future work

While the proposed user support system proved to be able to recommend favorable scan parameters, many error sources remain and should be addressed by future work.

- **Further scan parameters for gaining knowledge:** The presented experiments focused on scan parameters related to the x-ray source. However, additional other parameters influence the measurement results [2]. For example, the workpiece orientation may have a significant impact on the measurement results [14, 25]. Also, the number of projections can be an effective way to reduce measurement time [26]. These factors could all be included in future experimental designs. In this study, they were omitted due to limited measurement capacity of our laboratory. Of note, our approach already depended on performing more than 300 CT experiments (180 for the experimental design alone without repetitions).
- **Global surface determination procedure:** In this work, we used VG Studio's standard algorithm for surface determination to evaluate the experiments. It is known that local-adaptive surface determination can lead to smaller uncertainties and lower systematic errors. Of note, the presented experiments' aim was to highlight the difference caused by using different scan parameters in respect to the measurement results. Using the standard surface determination algorithm highlighted the differences between well- and ill-chosen scan parameters more clearly than local-adaptive surface determination would have.
- **VDI/VDE 2630 2.1-based approach:** To ensure practical feasibility of the presented experimental study, we had to modify the approach described in VDI/VDE 2630 2.1 to reduce the number of measurement repetitions to determine systematic errors and the measurement uncertainty. Consequentially, we used the measurement deviation to estimate the systematic error. The results show that this simplification is feasible, as the aggregated features' measurement deviations were significantly larger than their mean uncertainty values (compare results of V_U and V_b). Additionally, we considered the measurement uncertainty values to determine which scan parameters led to optimal results. Accordingly, we designed the evaluation to acknowledge that the systematic errors calculated from our modified approach only represented measurement deviations.
- **Quality index:** We calculated the quality index Q by aggregating measurement results from different measurement features. Our aggregation procedure assumes that users prefer scan parameters that lead to the most accurate measurement when considering all measurement features. However, for more specialized tasks, the results of single features could be considered to derive the CBR system's cases rather than the quality index Q.
- **Case labeling by size and material:** The CBR system only uses a workpiece's size and material to determine which cases to retrieve from the database. For larger, more powerful and therefore more complex CT systems, more complex matching equations may be necessary to achieve satisfactory results. For example, for a more complex system, it could be necessary to separate between workpiece size and penetration length to improve results.
- **Further attributes in CBR system:** Including further identification attributes to the CBR system is possible by extending the matching equation (equation 8). Binary categories such as the type of feature could be included by introducing if-then-constraints, while non-binary categories like the penetration length could be represented by additional parameters.
- **Alternative to revising cases:** In its current version, the CBR system relies on the user to perform tactile reference measurements to revise new cases (section 3.2.3). This is time consuming. To overcome this hurdle, we propose to investigate a connection between the image quality and the measurement results. We propose to derive statistical or machine learning models that predict metrological values such as the systematic error purely based on the reconstructions' image quality by reevaluating the experiments of this study accordingly. However, first, suitable imaging parameters need to be identified and verified. Previous work by Kramer *et al* [10] or Reiter *et al* [27, 28] could serve as a starting point.
- **Resolution parameter:** The resolution parameter allowed an in-depth interpretation of the measurement results. However, the resolution parameter was difficult to interpret for parts made of plastic. This could be attributed to manufacturing tolerances, which resulted from the comparatively complex process of milling a sphere-shaped feature to a plastic part. An adaption of another technique to determine

the resolution, e.g. by analyzing the modulation transfer function according to ASME 1695 [29], could be considered for future work.

Data availability statement

The data that support the findings of this study are openly available at the following URL/DOI: 10.35097/537.

Acknowledgments

ORCID iDs

Leonard Schild ⬤ https://orcid.org/0000-0001-5656-8779
Katja Höger ⬤ https://orcid.org/0000-0003-3235-6258
Simone Carmignato ⬤ https://orcid.org/0000-0001-6135-6834

References

[1] Buratti A, Bredemann J, Pavan M and Schmitt R Applications of CT for dimensional metrology 2018 S Carmignato, W Dewulf and R Leach (eds) *Industrial X-Ray Computed Tomography* (Cham: Springer) pp 333–69

[2] Dewulf W, Bosse H, Carmignato S and Leach R 2022 Advances in the metrological traceability and performance of x-ray computed tomography *CIRP Ann.* **71** 693–716

[3] Stolfi A, De Chiffre L and Kasperl S 2018 Error Sources *Industrial X-Ray Computed Tomography* ed S Carmignato, W Dewulf and R Leach (Cham: Springer) pp 143–84

[4] Carmignato S 2012 Accuracy of industrial computed tomography measurements: experimental results from an international comparison *CIRP Ann.* **61** 491–4

[5] Stolfi A and de Chiffre L 2018 Interlaboratory comparison of a physical and a virtual assembly measured by CT *Precis. Eng.* **51** 263–70

[6] Schmitt R, Isenberg C and Niggemann C 2012 Knowledge-based system to improve dimensional CT measurements *4th Conf. on Industrial Computed Tomography (ICT) 2012: Proc.*

[7] Buratti A, Achour S and Schmitt R Optimisation of Workpiece Manipulation for Multimaterial Measurements in Industrial Computed Tomography 2016 ed P Bointon, R Leach and N Southon *Proc. 16th Euspen International Conf.* (*Nottingham, UK*) pp 105–6

[8] Buratti A, Grozmani N, Voigtmann C, Sartori L V and Schmitt R 2018 Determination of the optimal imaging parameters in industrial computed tomography for dimensional measurements on monomaterial workpieces *Meas. Sci. Technol.* **29** 115009

[9] Schmitt R H, Buratti A, Grozmani N, Voigtmann C and Peterek M 2018 Model-based optimisation of CT imaging parameters for dimensional measurements on multimaterial workpieces *CIRP Ann.* **67** 527–30

[10] Krämer A, Böhmler P and Lanza G 2016 Optimierung von Aufnahmeparametern mittels projektionsbasierter Qualitätskenngrößen in der industriellen Computertomographie ed *GMA/ITG-Fachtagung Sensoren Und Messsysteme: Proc.* AMA Verband für Sensorik und Messtechnik e.V. 18 pp 383–90

[11] Christoph R, Leinweber C, Fischer A, Weise H and Kachelrieß M 2019 Validation of a method for the optimization of scan parameters for measuring with computed tomography *9th Conf. on Industrial Computed Tomography (ICT) 2019: Proc.*

[12] Reisinger S, Kasperl S, Franz M, Hiller J and Schmid U 2011 Simulation-based planning of optimal conditions for industrial computed tomography *Int. Symp. on Digital Industrial Radiology and Computed Tomography: Proc.*

[13] Reiter M, Erler M, Kuhn C, Gusenbauer C and Kastner J 2016 SimCT: a simulation tool for x-ray imaging *6th Conf. on Industrial Computed Tomography (ICT) 2016: Proc.*

[14] Xue L, Suzuki H, Ohtake Y, Fujimoto H, Abe M, Sato O and Takatsuji T 2016 Quality evaluation of x-ray computed tomography volume data in dimensional metrology *6th Conf. on Industrial Computed Tomography (ICT) 2016: Proc.*

[15] Schielein R, Scholz G, Wagner R, Kretzer C, Fuchs T, Kasperl S and Bär F 2016 The MUSICES project: simulative automated CT acquisition planning for historical brass instruments improves image quality *6th Conf. on Industrial Computed Tomography (ICT) 2016: Proc.*

[16] Giedl-Wagner R, Miller T and Sick B 2012 Determination of optimal CT scan parameters using radial basis function neural networks *4th Conf. on Industrial Computed Tomography (ICT) 2012: Proc.*

[17] Montani S and Jain L C 2014 *Successful Case-Based Reasoning Applications-2* 1st edn (Heidelberg: Springer) (https://doi.org/10.1007/978-3-642-38736-4)

[18] Beierle C and Kern-Isberner G 2019 *Methoden wissensbasierter Systeme: Grundlagen, Algorithmen, Anwendungen (Computational Intelligence)* 6th edn (Wiesbaden: Springer Fachmedien Wiesbaden) (https://doi.org/10.1007/978-3-658-27084-1)

[19] Fleßner M, Müller A, Helmecke E and Hausotte T 2015 Automated detection of artefacts for computed tomography in dimensional metrology *Int. Symp. on Digital Industrial Radiology and Computed Tomography (DIR 2015): Proc.* (available at: www.vdi.de/richtlinien/details/vdivde-2630-blatt-21-computertomografie-in-der-dimensionellen-messtechnik-bestimmung-der-messunsicherheit-und-der-pruefprozesseignung-von-koordinatenmessgeraeten-mit-ct-sensoren)

[20] VDI/VDE 2630 Blatt 2.1 - 2015 Computed tomography in dimensional measurement - Determination of the uncertainty of measurement and the test process suitability of coordinate measurement systems with CT sensors

[21] Schmitt R and Niggemann C 2010 Uncertainty in measurement for x-ray-computed tomography using calibrated work pieces *Meas. Sci. Technol.* **21** 54008

[22] Müller P, Hiller J, Dai Y, Andreasen J L, Hansen H N and de Chiffre L 2014 Estimation of measurement uncertainties in x-ray computed tomography metrology using the substitution method *CIRP J. Manuf. Sci. Technol.* **7** 222–32

[23] Zanini F and Carmignato S 2017 Two-spheres method for evaluating the metrological structural resolution in dimensional computed tomography *Meas. Sci. Technol.* **28** 114002

[24] Hermanek P and Carmignato S 2017 Porosity measurements by x-ray computed tomography: accuracy evaluation using a calibrated object *Precis. Eng.* **49** 377–87

[25] Villarraga-Gómez H, Amirkhanov A, Heinzl C and Smith S T 2021 Assessing the effect of sample orientation on dimensional x-ray computed tomography through experimental and simulated data *Measurement* **178** 109343

[26] Villarraga-Gómez H and Smith S T 2020 Effect of the number of projections on dimensional measurements with x-ray computed tomography *Precis. Eng.* **66** 445–56

[27] Reiter M, Krumm M, Kasperl S, Kuhn C, Erler M, Weiss D, Heinzl C, Gusenbauer C and Kastner J 2012 Evaluation of transmission based image quality optimisation for x-ray computed *4th Conf. on Industrial Computed Tomography (ICT) 2012: Proc.* pp 241–50

[28] Reiter M, Weiss D, Gusenbauer C, Erler M, Kuhn C, Kasperl S and Kastner J 2014 Evaluation of a histogram-based image quality measure for x-ray computed tomography *5th Conf. on Industrial Computed Tomography (ICT) 2014: Proc.*

[29] ASTM E1695-20 Test method for measurement of computed tomography (CT) system performance (available at: www. astm.org/e1695-20e01.html)